ASCE Journal of Geotechnical and Geoenvironmental Engineering

# Effects of Pillar Depth and Shielding on the Interaction of Crossing Multitunnels

Charles W. W. Ng, Thayanan Boonyarak, and David Mašín

**DOI:** 10.1061/(ASCE)GT.1943-5606.0001293

## Supplemental Data

# Table of contents

# CHAPTER 1
# ADDITIONAL DETAILS OF CENTRIFUGE MODELING

## 1.1 Introduction

This chapter provides additional details of centrifuge modeling to enhance the clarity the manuscript entitled "Effects of pillar depth and shielding on the interaction of crossing multitunnels". Detailed model preparation and instrumentation are described in this document.

## 1.2 Model Preparation

Heavy fluid was filled in the "donuts" in the new tunnel in each test as shown in Figure S1a. Temporary support was used to place the new tunnel in the specified location.

Dry silica Toyoura sand was used in each centrifuge test. The average particle size ($D_{50}$), maximum void ratio ($e_{max}$), minimum void ratio ($e_{min}$), specific gravity ($G_s$) and critical state internal friction angle ($\phi_c$) of Toyoura sand are 0.17 mm, 0.977, 0.597, 2.64 and 30°, respectively (Ishihara, 1993). Grain size effects on soil-tunnel interaction were considered insignificant when the ratio of tunnel diameter to average particle size was larger than 175 (Garnier et al., 2007). In this study, the ratio of model tunnel diameter (100 mm) to average particle size (0.17 mm) was 588.

A dry pluviation technique was adopted to prepare the soil sample in each test. A drop height of 500 mm and a pluviation rate of about 100 kg/hour were used to control the density of the soil sample.

Each tunnel was placed after the level of pluviated sand reached the designed height. By using some thin wires and a temporary structural beam above, the new tunnel was "wished-in-place" in position (see Figure S1b). These wires and the beam were removed after the pluvial deposition reached the bottom of the new tunnel to support it.

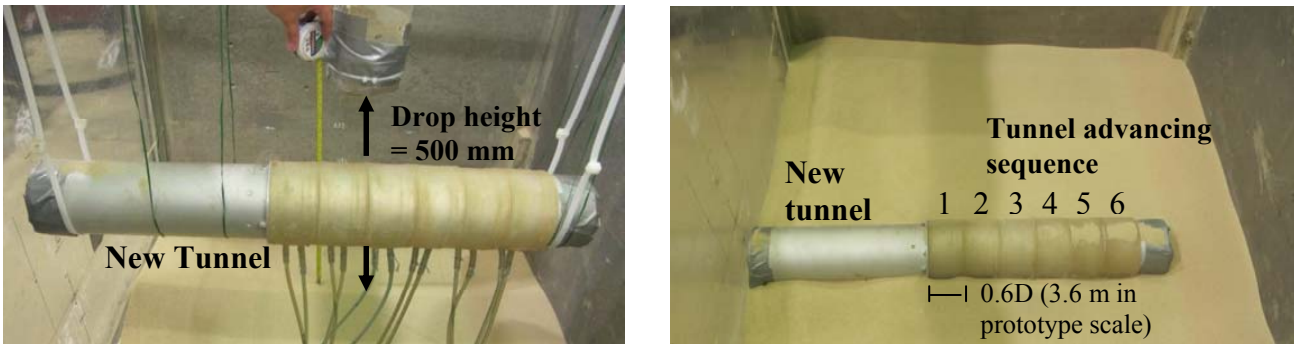


(a) (b)

**Figure S1** (a) Preparation of the new tunnel; (b) tunnel advancing sequence in a centrifuge test

# 1.3 Instrumentation

Figure S2 shows the types and locations of instruments installed in the existing tunnel. To measure tunnel settlement, linear variable differential transformers (LVDTs) were connected to the crown of the existing tunnel at various points via extension rods.

Each extension rod was made of an aluminum alloy housed in a hollow aluminum alloy tube in order to reduce friction with the surrounding soil. In Test E2N3, the LVDTs measuring settlement of the existing tunnel were all installed along one half of that tunnel and the maximum distance of the extension rods from the centerline of the new tunnel was 4D (see Fig. S3). In Tests E2N5 and E2,3N5, the extension rods were placed along the length of the existing tunnel and were within a distance of 3D from the centerline of the new tunnel. The LVDTs were arranged differently in Tests E2N5 and E2,3N5 to observe the response of the existing tunnel near the centerline of the new tunnel, where maximum tunnel settlement was expected to occur.

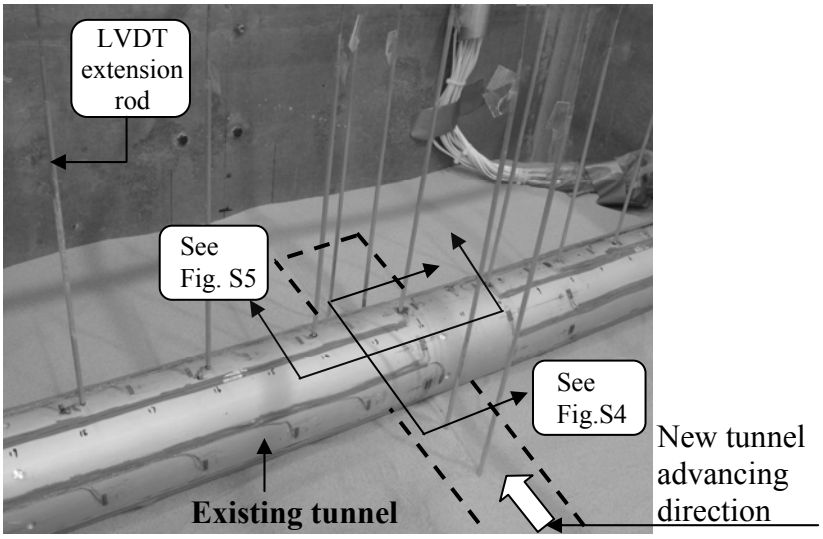


**Figure S2** Instruments installed at the existing tunnel

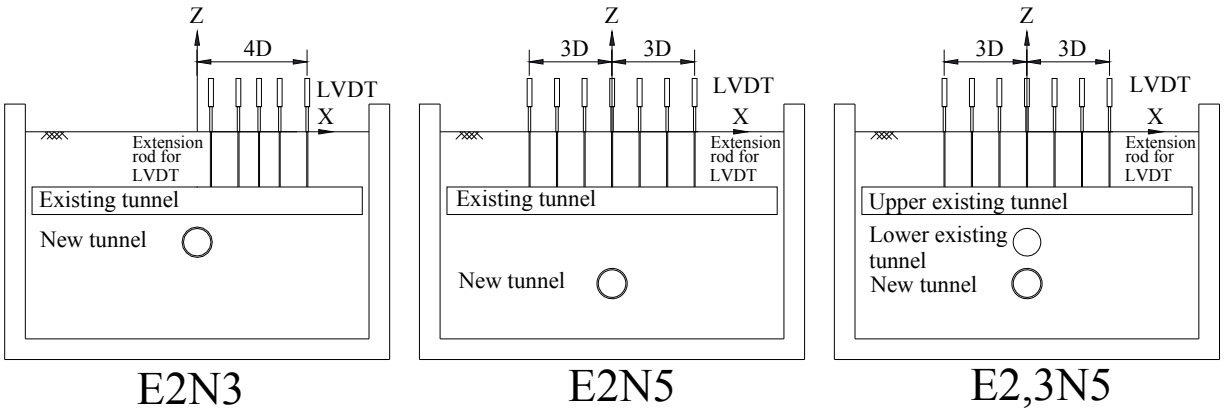


**Figure S3** Arrangement of extension rods for LVDT in each test

Figure S4 shows potentiometers installed inside the existing tunnel at the location directly above the new tunnel. Four potentiometers were placed at the crown, at each springline and at the invert to measure tunnel deformation. A potentiometer is a three-terminal resistor that measures a change in resistance with a change in the travel distance of a slider (Todd, 1975). The accuracy of the potentiometers used in this study was estimated to be within ±0.017 mm in model scale (equivalent to ±1 mm in prototype scale) by considering the standard deviation of the data once the centrifugal acceleration had reached 60g prior to tunnel excavation.

Eight sets of foil strain gages were attached to both inner and outer surfaces of the lining of the existing tunnel at a spacing of about 45° around of the circumference. The strain gages having a gage factor of 2 were connected into a full Wheatstone bridge to compensate for temperature effects. In Test E2,3N5, potentiometers and strain gages in the transverse direction were also installed in the lower existing tunnel at the location directly below the upper existing tunnel.

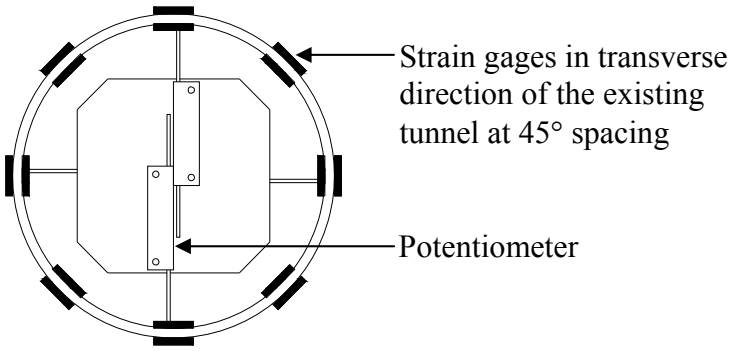


**Figure S4** Transverse section view of the existing tunnel

Figure S5 shows a typical longitudinal section view of the existing tunnel. Four potentiometers were mounted on a plate, which was connected to a frame that was fixed to the lining of the existing tunnel. A total of 19 sets of semiconductor strain gages were attached along the length of the existing tunnel at the crown and invert at a typical spacing of 50 mm. The strain gages in the longitudinal direction of the existing tunnel were connected into a full Wheatstone bridge, having a gage factor of 140. Different types of strain gages were used in the longitudinal and transverse directions of the existing tunnel because the semiconductor ones are easily damaged during installation and so cannot be attached to the inner surface of the tunnel lining.

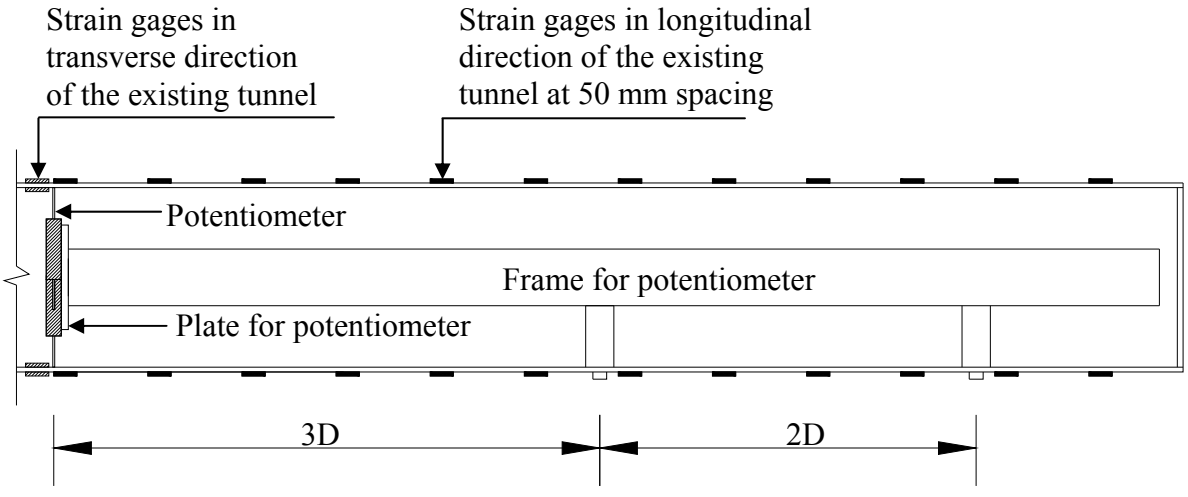


**Figure S5** Longitudinal section view of the existing tunnel

# CHAPTER 2

# PLAXIS IMPLEMENTATION OF HYPOPLASTICITY

## 2.1 Introduction

This chapter provides general information related to the Hypoplasticity model. General equations, time integration, input parameters, trouble shooting and evaluation of the model are described in this chapter.

## 2.2 Hypoplasticity

Hypoplasticity is a particular class of incrementally non-linear constitutive models, developed specifically to predict the behavior of soils. The basic structure of the hypoplastic models has been developed during 1990's at the University of Karlsruhe. In hypoplasticity, unlike in elasto-plasticity, the strain rate is not decomposed into elastic and plastic parts, and the models do not use explicitly the notions of the yield surface and plastic potential surface. Still, the models are capable of predicting the important features of the soil behavior, such as the critical state, dependency of the peak strength on soil density, non-linear behavior in the small and large strain range, dependency of the soil stiffness on the loading direction, etc.

This is achieved by the hypoplastic equation being non-linear in the stretching tensor **D**. The basic hypoplastic equation may be written as

$$\mathring{\mathbf{T}} = \boldsymbol{L} : \mathbf{D} + \mathbf{N}\,\|\mathbf{D}\| \qquad \text{(S1)}$$

where $\mathring{\mathbf{T}}$ is the objective (Jaumann) stress rate, **D** is the Euler's stretching tensor and $\boldsymbol{L}$ and **N** are fourth- and second order constitutive tensors, respectively. The early hypoplastic models were developed by trial and error, by choosing suitable candidate functions from the most general form of isotropic tensor-valued functions of two tensorial arguments (Kolymbas, 1991). An important step forward in developing the hypoplastic model was the implementation of the critical state concept. Gudehus (1996) proposed a modification of Equation (S1) to include the influence of the stress level (barotropy) and the influence of density (pyknotropy). The modification equation reads

$$\mathring{\mathbf{T}} = f_s \boldsymbol{L} : \mathbf{D} + f_s f_d \mathbf{N}\,\|\mathbf{D}\| \qquad \text{(S2)}$$

Here $f_s$ and $f_d$ are scalar factors expressing the influence of barotropy and pyknotropy. The model by Gudehus (1996) was later refined by von Wolffersdorff (1996) to incorporate Matsuoka-Nakai critical state stress condition. This model is nowadays considered as a standard hypoplastic model for granular materials, and this version is also implemented in PLAXIS.

Later developments focused on the development of hypoplasticity for fine grained soils. Herle and Kolymbas (2004) modification the model by von Wolffersdorff (1996) to allow for lower friction angles and independent calibration of bulk and shear stiff Based on this model, and the "Generalized hypoplasticity" principle by Niemunis (2002), Mašín (2005) developed a model for clays characterized by a simple calibration procedure and capability

of correct predicting the very small strain behavior (in combination with the "intergranular strain concept" described later). This clay version is incorporated in PLAXIS. Later on, Mašín (2007) proposed modification of the model from Mašín (2005) to consider the behavior of clays with meta-stable structure. This model is also available in PLAXIS.

The basic hypoplastic models characterized by Eq. (S2) predict successfully the soil behavior in the medium to large strain range. However, in the small strain range and upon cyclic loading they fail in predicting the high quasi-elastic soil stiffness. To overcome this problem, Niemunis and Herle (1997) proposed an extension of the hypoplastic equation by considering additional state variable "Intergranular strain" determine the direction of the previous loading. This modification often denoted as the "Intergranular strain concept", is implemented in PLAXIS and can be used with both the model for granular materials and the model for clays.

The rate formulation of the enhanced model is given by

$$\mathring{\mathbf{T}} = \boldsymbol{M} : \mathbf{D} \qquad \text{(S3)}$$

where $\boldsymbol{M}$ is the fourth-order tangent stiffness tensor of the material. The total strain can be thought of as the sum of a component related to the deformation of interface layers at intergranular contacts, quantified by the intergranular strain tensor $\boldsymbol{\delta}$; and a component related to the rearrangement of the soil skeleton. For reverse loading conditions and neutral loading conditions the observed overall strain is related only to the deformation of the intergranular interface layer and the soil behavior is hypoelastic, whereas in continuous loading conditions the observed overall response is also affected by particle rearrangement in the soil skeleton and the soil behavior is hypoplastic.

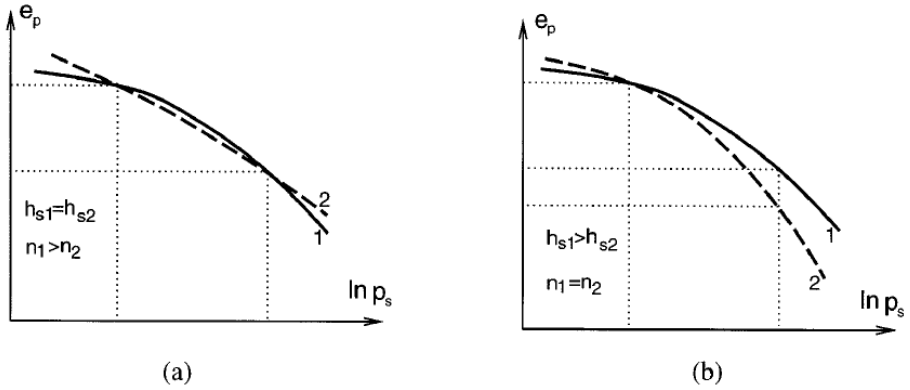


**Figure S6** Influence of $n$ (a) and $h_s$ (b) on oedometric curves (Herle and Gudehus, 1999).

### 2.2.1 Hypoplastic model for granular materials

The hypoplastic model for granular materials has eight material parameters - $\varphi_c$, $h_s$, $n$, $e_{d0}$, $e_{c0}$, $e_{i0}$, $\alpha$ and $\beta$. Their calibration procedure has been detailed by Herle and Gudehus (1999). A somewhat simplified calibration procedure is described in the following. The critical state friction angle $\varphi_c$ can be obtained directly by the measurement of the angle of repose. The next two parameters $h_s$ and $n$ can be directly computed from oedometric loading curves. The parameter $n$ controls the curvature of oedometric curve and $h_s$ controls the overall slope of oedometric curve as is shown in Figs S6 (a) and (b). Having two states at the

oedometric curve (Fig. S6), the parameter $n$ can be calculated from

$$n = \frac{\ln(e_{p1}C_{c2}/e_{p2}C_{c1})}{\ln(p_{s2}/p_{s1})} \tag{S4}$$

where mean stresses $p_{s1}$ and $p_{s2}$ can be calculated from axial stresses using the Jáky formula $K_0 = 1 - \sin\varphi_c$, and $e_{p1}$ and $e_{p2}$ are the void ratios corresponding to the stresses $p_{s1}$ and $p_{s2}$. Tangent compression indices corresponding to the limit values of the interval $p_{s1}$ and $p_{s2}$ ($C_{c1}$ and $C_{c2}$) can be approximated by secant moduli between loading steps preceding and following the steps $p_{s1}$ and $p_{s2}$. The parameter $h_s$ can then be obtained from

$$h_s = 3p_s \left(\frac{ne_p}{C_c}\right)^{1/n} \tag{S5}$$

where $C_c$ is a secant compression index calculated from limit values of the calibration interval $p_{s1}$ and $p_{s2}$; $p_s$ and $e_p$ are averages of the limit values of $p$ and $e$ for this interval.

The next three model parameters are the reference void ratios $e_{d0}$, $e_{c0}$ and $e_{i0}$, corresponding to the densest, critical state and loosest particle packing at the zero mean stress. The reference void ratios $e_d$, $e_c$ and $e_i$ corresponding to the non-zero stress depend on the mean stress by formula due to Bauer (1996):

$$e_c = e_{c0} \exp\left[-\left(\frac{3p}{h_s}\right)^n\right] \tag{S6}$$

The dependency of the reference void ratios on the mean stress is demonstrated in Fig. S7.

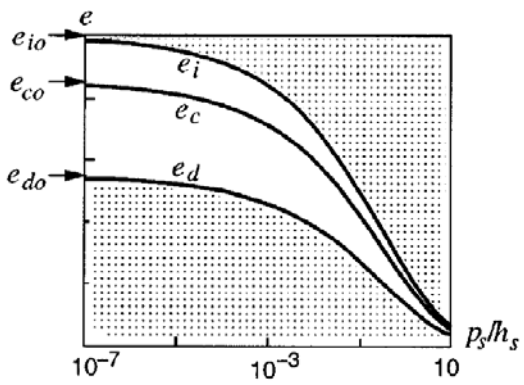


**Figure S7** The dependency of the reference void ratios $e_{d0}$, $e_{c0}$ and $e_{i0}$ on the mean stress (Herle and Gudehus, 1999 ).

Following Herle and Gudehus (1999), initial void ratio $e_{max}$ of a loose oedometric specimen can be considered equal to the critical state void ratio at zero pressure $e_{c0}$. Void ratios $e_{d0}$ and $e_{i0}$, which are the next two parameters, can approximately be obtained from empirical

relations. The physical meaning of $e_{d0}$ is void ratio at maximum density, void ratio $e_{i0}$ represents intercept of the isotropic normal compression line with $p = 0$ axis. Void ratio $e_{i0}$ can be obtained by multiplication $e_{c0}$ by a factor 1.2. The ratio $e_{i0}/e_{c0} \approx 1.2$ was derived by Herle and Gudehus (1999) considering skeleton consisting of ideal spherical particles.

The minimum void ratio $e_{d0}$ should be obtained by densification of a granular material by means of cyclic shearing with small amplitude under constant pressure. If such a test is not available, it can be approximated using an empirical relation, with

$$e_{d0}/e_{c0} \approx 0.4$$

The last two parameters $\alpha$ and $\beta$ should be calibrated by means of single-element simulations of the drained triaxial tests. The two parameters control independently different aspects of soil behavior, namely the parameter $\beta$ controls the shear stiffness and $\alpha$ controls the peak friction angle.

For further details on model calibration, see Mašín (2010).

### 2.2.2 Hypoplastic model for clays

The basic model Mašín (2005) requires five parameters ($N$, $\lambda^*$, $\kappa^*$, $\phi_c$ and $r$). The parameters have the same physical interpretation as parameters of the Modified Cam clay model, and they are thus easy to calibrate based on standard laboratory experiments. The model parameters $N$ and $\lambda^*$ define the position and the slope of the isotropic normal compression line in the $\ln(1 + e)$ vs. $\ln p$ plane:

$$\ln(1 + e) = N - \lambda * \ln (p/pr) \qquad \text{(S7)}$$

where $p_r = 1$ kPa is a reference stress; parameter $\kappa^*$ defines the slope of the isotropic unloading line in the same plane. Their definition is demonstrated in Fig. S8 and their calibration using isotropic loading and unloading tests on reconstituted London Clay specimens by Gasparre (2005) is demonstrated in Fig.S9 (Mašín, 2009). The last two parameters are the critical state friction angle $\phi_c$ and the parameter $r$ that controls the shear stiffness. Due to the non-linear nature of the model, the parameter $r$ needs to be calibrated by simulation of the laboratory experiments. With decreasing value of $r$ the shear stiffness is increasing (Fig. S9b).

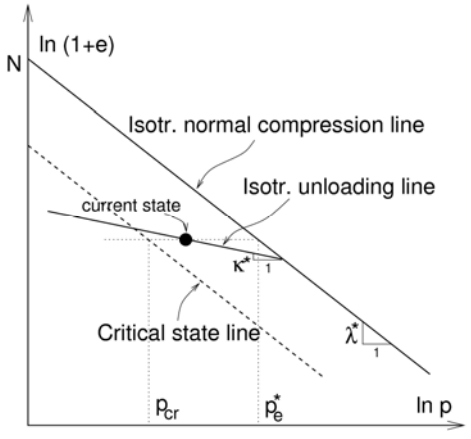


**Figure S8** Definition of parameters $N$, $\lambda^*$ and $\kappa^*$.

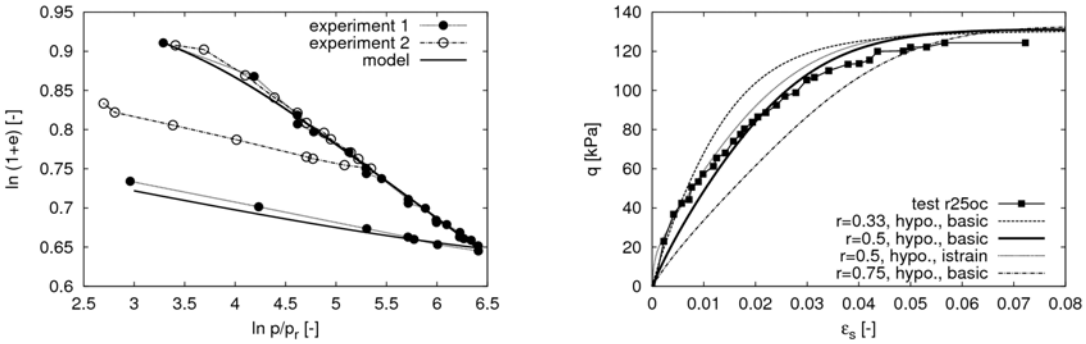


**Figure S9** (a) Calibration of parameters $N$, $\lambda^*$ and $\kappa^*$ using isotropic tests on reconstituted London clay, (b) calibration of the parameter $r$ using undrained shear test on reconstituted London clay (exp. data from Gasparre,2005).

For details of the model for clays with meta-stable structure, see Mašín (2007). Calibration procedure is also described in detail in Mašín (2010).

## 2.2.3 The intergranular strain concept (small strain behavior)

The intergranular strain concept requires five additional parameters: $R$ controlling the size of the elastic range, $\beta_r$ and $\chi$ controlling the rate of stiffness degradation, $m_R$ controlling the initial shear stiffness for the initial and reverse loading conditions and $m_T$ controlling the stiffness upon neutral loading conditions. When combined with the hypoplastic model for clays, the initial very-small-strain shear stiffness $G_0$ may be calculated from

$$G0 \cong m_R.p/(r.\lambda^*) \qquad \text{(S8)}$$

The parameters should be calibrated by simulating the laboratory experiments with measurements of the small strain stiffness using local strain transducers and with measurements of the very-small-strain stiffness using dynamic methods (such as bender elements). The influence of the parameter $m_R$ and $\beta_r$ on the predicted small-strain shear stiffness curves is demonstrated in Fig. S10.

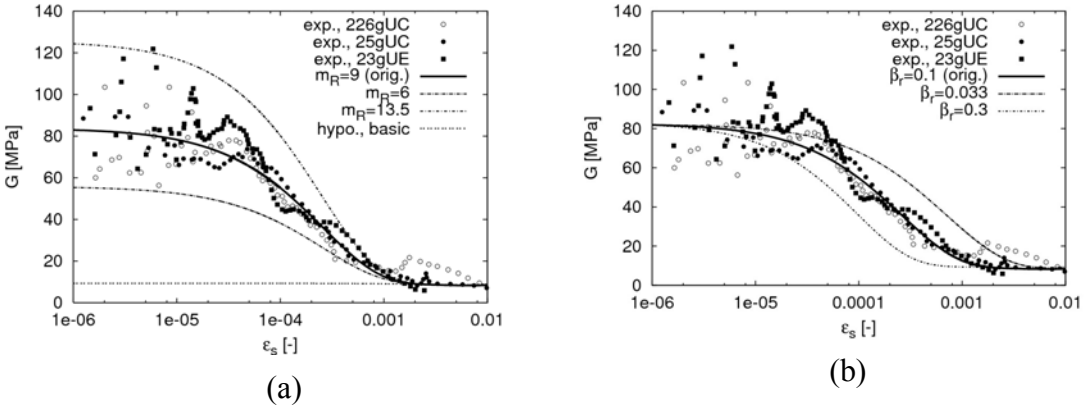


(a) (b)

**Figure S10** The influence of the parameters $m_R$ and $\beta_r$ on the predicted small-strain stiffness behavior (experimental data from Gasparre, 2005)

### 2.2.3 Hypoplastic model for unsaturated soils

The implementation contains a model for unsaturated soils by Mašín and Khalili (2008). See the journal publication for more information about the model. If the journal access is not available to you, request a copy from Mašín http://www.natur.cuni.cz/masin

## 2.3 Time integration

Constitutive models are integrated using explicit adaptive integration scheme with local substepping. The constitutive model forms an ordinary differential equation of the form

$$dy/dt = f(t,y)$$

The equation is for finite time step size $\Delta t$ solved using the Runge-Kutta method. Solutions that correspond to the second- and third- order accuracy of Taylor series expansion are given by

$$y^{(2)}_{(t+\Delta t)} = y_{(t)} + k_2$$

$$y^{(3)}_{(t+\Delta t)} = y_{(t)} + \frac{1}{6}(k_1 + 4k_2 + k_3)$$

where

$$k_1 = \Delta t \; f\left(t, y_{(t)}\right)$$

$$k_2 = \Delta t \; f\left(t + \frac{\Delta t}{2}, y_{(t)} + \frac{k_1}{2}\right)$$

$$k_3 = \Delta t \; f\left(t + \Delta t, y_{(t)} - k_1 + 2k_2\right)$$

The accuracy of the solution is estimated following Fehlberg as the difference between the second- and third- order solutions. The time step size $\Delta t$ is accepted, if

$$err = \left\| y^{(3)}_{(t+\Delta t)} - y^{(2)}_{(t+\Delta t)} \right\| < TOL$$

where TOL is a prescribed error tolerance. If the step-size $\Delta t$ is accepted, $y^{(3)}_{(t+\Delta t)}$ is considered as a solution for the given time step and the new time step size $\Delta t^n$ is estimated according to Hull

$$\Delta tn = \min[4\Delta t, 0.9\Delta t \, (TOL/err)^{(1/3)}]$$

If the step-size $\Delta t$ is not accepted, the step is re-computed with new time step size

$$\Delta tn = \max[\Delta t/4, 0.9\Delta t \, (TOL/err)^{(1/3)}]$$

In the case the prescribed minimum time step size or the prescribed maximum number of time substeps is reached, the finite element program is asked to reject the current step and to decrease the size of the global time step.

# 2.4 Input of parameters and state variables in PLAXIS

## 2.4.1 Hypoplastic model for granular materials

Parameters are specified in the PLAXIS input in the following order:

- Parameter 1 – critical state friction angle $\phi_c$
- Parameter 2 – $p_t$ – shift of the mean stress due to cohesion. The effective stress $\boldsymbol{\sigma}$ used in the model formulation is replaced by $\boldsymbol{\sigma} - \mathbf{1}p_t$. Non-zero value of $p_t$ is needed to overcome problems with stress-free state. If $p_t = 0$, it will be replaced by a default value of 10 kPa. Any other value can be input by user (for basic hypoplasticity, set $p_t$ to very low number, e.g. $p_t = 1.e-5$)
- Parameters 3-9 – parameters of the basic hypoplastic model for granular materials $h_s$, $n$, $e_{d0}$, $e_{c0}$, $e_{i0}$, $\alpha$, $\beta$
- Parameters 10-14 – the intergranular strain concept parameters ($m_R$, $m_T$, $R$, $\beta_r$, $\chi$). If $m_R = 0$ the intergranular strain concept is switched off and the problem is simulated using the basic hypoplastic model
- Parameter 15 – not used
- Parameter 16 – initial void ratio corresponding to the zero mean stress $e_0$ or initial void ratio $e$. If $Par(16) < 10$, then $e$ is calculated from the mean stress $p$ and from $e_0 = Par(16)$ using Bauer (1996) formula. If $Par(16) > 10$, then $e = Par(16) - 10$
- Parameters 17-22 – initial values of the intergranular strain tensor $\boldsymbol{\delta}$ in Voigt notation ($\delta_{11}$, $\delta_{22}$, $\delta_{33}$, $2\delta_{12}$, $2\delta_{13}$, $2\delta_{23}$)

**State variables:**

The routine uses 14 state variables:

- State v. 1-6 – intergranular strain tensor $\boldsymbol{\delta}$ in Voigt notation ($\delta_{11}, \delta_{22}, \delta_{33}, 2\delta_{12}, 2\delta_{13}, 2\delta_{23}$)
- State v. 7 – void ratio $e$
- State v. 8 – not used
- State v. 9 – Effective mean stress
- State v. 10 – Number of evaluation of the constitutive model in one global time step (for postprocessing only)
- State v. 11 – Mobilized friction angle $\phi_{mob}$ in degrees (for postprocessing only)
- State v. 12 – Normalized length $\rho$ of the intergranular strain tensor $\delta$ (for postprocessing only)
- State v. 13 – Suggested size of the first time substep (for calculation control)
- State v. 14 – free

The hypoplastic model for granular materials is implemented via user define subroutine usermod.dll. To use the model in PLAXIS, copy the file UsrMod.dll into the PLAXIS installation directory. Then, select "User-defined model" from the Material model combo box in the General tab sheet (Fig. S11). After selecting the user-define model, correct user-define dynamic library (typically UsrMod.dll) needs to be selected in the "Available DLL's" combo box under "Parameters" tab sheet. In the "Models in DLL" combo box, model with ID 1 (Hypoplas.-sand) must be selected. The parameters can then be input into the parameter table (Fig. S12).

Parameters of the sand hypoplastic model for diff t soils have been evaluated by Herle and Gudehus (1999). They are given in Table S1. Parameters of the intergranular strain concept for granular materials are in Tab. S2.

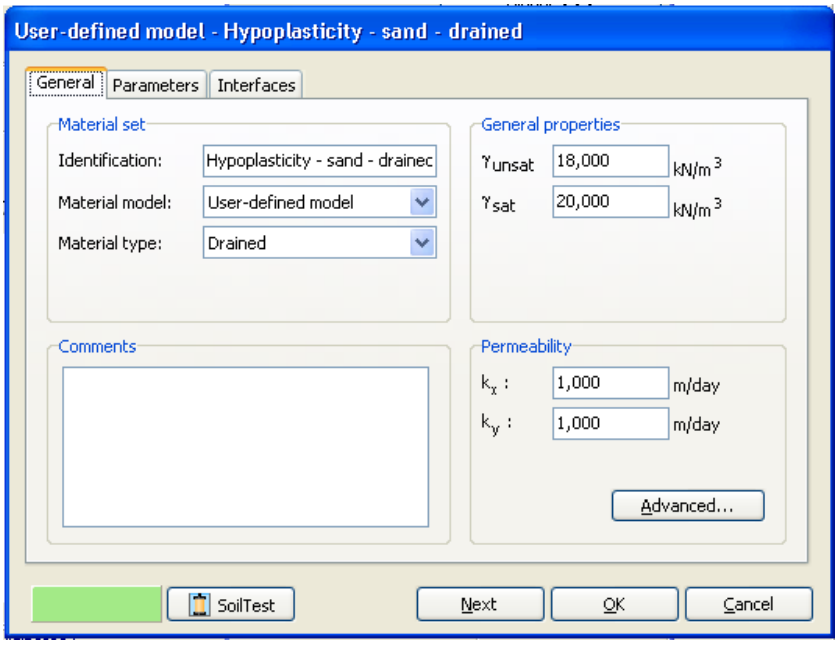


**Figure S11** Selecting user defined model in the Material model combo box.

## 2.4.2 Hypoplastic model for clays

Parameters are specified in the PLAXIS input in the following order:

**Parameters:**

- Parameter 1 – critical state friction angle $\phi_c$
- Parameter 2 – $p_t$ – shift of the mean stress due to cohesion. The effective stress $\boldsymbol{\sigma}$ used in the model formulation is replaced by $\boldsymbol{\sigma} - \mathbf{1}p_t$. Non-zero value of $p_t$ is needed to overcome problems with stress-free state. If $p_t = 0$, it will be replaced by a default value of 10 kPa. Any other value can be input by user (for basic hypoplasticity, set $p_t$ to very low number, e.g. $p_t = 1.e-5$)

- Parameters 3-6 – parameters of the basic hypoplastic model for clays $\lambda^*$, $\kappa^*$, $N$, $r$
- Parameters 7-9 – parameters of the model for clays with meta-stable structure ($k$, $A$ and $s_f$)

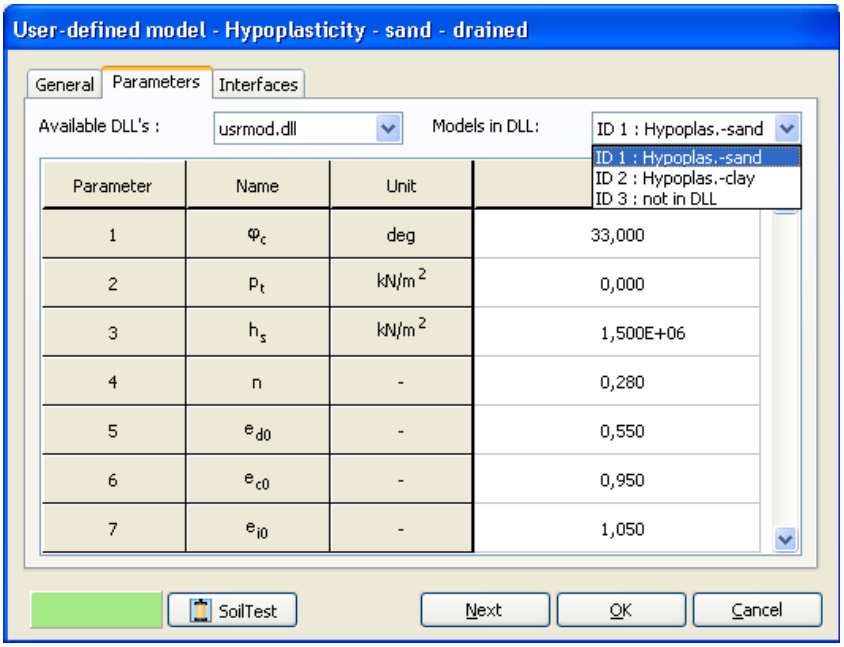


**Figure S12** Selecting sand hypoplasticity model in the "Parameters" tab sheet.

- Parameters 10-14 – the intergranular strain concept parameters ($m_R$, $m_T$, $R$, $\beta_r$, $\chi$). If $m_R$ = 0 the intergranular strain concept is switched off and the problem is simulated using the basic hypoplastic model.
- Parameter 15 – bulk modulus of water $K_w$ for undrained analysis using the penalty approach with user-define value of $K_w$. In drained analysis, consolidation analysis, and undrained analysis using PLAXIS option *undrained* $K_w$ should be set to 0.
- Parameter 16 – initial void ratio $e$ or overconsolidation ratio $OCR$. If $Par(16) < 10$, then $e = Par(16)$. If $Par(16) > 10$, then $OCR = Par(16) - 10$.
- Parameters 17-22 – initial values of the intergranular strain tensor $\boldsymbol{\delta}$ in Voigt notation ($\delta_{11}$, $\delta_{22}$, $\delta_{33}$, $2\delta_{12}$, $2\delta_{13}$, $2\delta_{23}$).
- Parameter 23 – initial value of sensitivity (model for clays with meta-stable structure). If $s = 0$, the basic model is used.

**State variables:**

The routine uses 14 state variables:

**Table S1** Typical parameters of the hypoplastic model for granular materials (Herle and Gudehus, 1999)

| Soil | $\phi_c$ | $h_s$ | $n$ | $e_{d0}$ | $e_{c0}$ | $e_{i0}$ | $\alpha$ | $\beta$ |
|---|---|---|---|---|---|---|---|---|
| Hochstetten gravel | 36° | 32 $\times 10^6$ kPa | 0.18 | 0.26 | 0.45 | 0.5 | 0.1 | 1.9 |
| Hochstetten sand | 33° | 1.5 $\times 10^6$ kPa | 0.28 | 0.55 | 0.95 | 1.05 | 0.25 | 1.5 |
| Hostun sand | 31° | 1.0 $\times 10^6$ kPa | 0.29 | 0.61 | 0.96 | 1.09 | 0.13 | 2 |
| Karlsruhe sand | 30° | 5.8 $\times 10^6$ kPa | 0.28 | 0.53 | 0.84 | 1 | 0.13 | 1 |
| Lausitz sand | 33° | 1.6 $\times 10^6$ kPa | 0.19 | 0.44 | 0.85 | 1 | 0.25 | 1 |
| Toyoura sand | | 2.6 $\times 10^6$ kPa | 0.27 | 0.61 | 0.98 | 1.1 | 0.18 | 1.1 |

**Table S2** Parameters of the intergranular strain concept for sandy soils (Niemunis and Herle, 1997)

| | $R$ | $m_R$ | $m_T$ | $\beta_r$ | $\chi$ |
|---|---|---|---|---|---|
| Hochstetten sand | 1.e-4 | 5.0 | 2.0 | 0.5 | 6 |

- State v. 1-6 – intergranular strain tensor $\boldsymbol{\delta}$ in Voigt notation ($\delta_{11}, \delta_{22}, \delta_{33}, 2\delta_{12}, 2\delta_{13}, 2\delta_{23}$)
- State v. 7 – void ratio $e$
- State v. 8 – sensitivity $s$ (for model with meta-stable structure)
- State v. 9 – Excess pore pressure $u$ for undrained analysis using user-defined value of $K_w$. In undrained analysis using PLAXIS option *undrained* this variable is equal to 0 end excess pore pressure may be found in standard PLAXIS menu
- State v. 10 – Effective mean stress
- State v. 11 – Number of evaluation of the constitutive model in one global time step (for postprocessing only)
- State v. 12 – Mobilized friction angle $\phi_{mob}$ in degrees (for postprocessing only)
- State v. 13 – Normalized length $\rho$ of the intergranular strain tensor $\boldsymbol{\delta}$ (for postprocessing only)

State v. 14 – Suggested size of the first time substep (for calculation control)

The hypoplastic model for granular materials is implemented via user define subroutine usermod.dll. To use the model in PLAXIS, copy the file UsrMod.dll into the PLAXIS installation directory. Then, select "User-defined model" from the Material model combo box in the General tab sheet (Fig. S11).

After selecting the user-define model, correct user-define dynamic library (typically UsrMod.dll) needs to be selected in the "Available DLL's" combo box under "Parameters"

tab sheet. In the "Models in DLL" combo box, model with ID 2 (Hypoplas.-clay) must be selected. The parameters can then be input into the parameter table (Fig. S13).

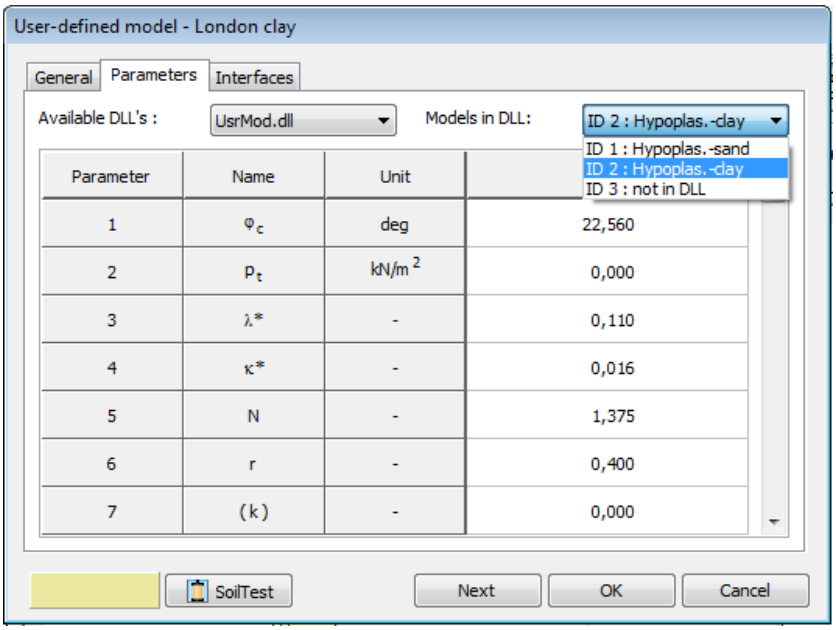


**Figure S13** Selecting clay hypoplasticity model in the "Parameters" tab sheet.

Parameters of the clay hypoplastic model for different soils have been evaluated by Mašín and co-workers. They are given in Table S3. Parameters of the model for clays with meta-stable structure are in Tab. S4 and typical parameters of the intergranular strain concept for fined grained soils are in Tab. S5.

## 2.4.3 Hypoplastic model for unsaturated soils

Parameters are specified in the PLAXIS input in the following order:

**Table S3** Typical parameters of the hypoplastic model for clays

| Soil | $\phi_c$ | $\lambda^*$ | $\kappa^*$ | $N$ | $r$ |
|---|---|---|---|---|---|
| London clay | 22.6◦ | 0.11 | 0.016 | 1.375 | 0.4 |
| Brno clay | 19.9◦ | 0.13 | 0.01 | 1.51 | 0.45 |
| Fujinomori clay | 34◦ | 0.045 | 0.011 | 0.887 | 1.3 |
| Bothkennar clay | 35◦ | 0.12 | 0.01 | 1.34 | 0.07 |
| Pisa clay | 21.9◦ | 0.14 | 0.01 | 1.56 | 0.3 |
| Beaucaire clay | 33◦ | 0.06 | 0.01 | 0.85 | 0.4 |
| Kaolin | 27.5◦ | 0.11 | 0.01 | 1.32 | 0.45 |
| London clay (data Gasparre) | 21.9◦ | 0.1 | 0.02 | 1.26 | 0.5 |
| Kaolin | 27.5◦ | 0.07 | 0.01 | 0.92 | 0.67 |
| Trmice clay | 18.7◦ | 0.09 | 0.01 | 1.09 | 0.18 |

**Table S4** Typical parameters of the model for clays with meta-stable structure

| Soil | $k$ | $A$ | $s_f$ |
|---|---|---|---|
| Pisa clay | 0.4 | 0.1 | 1 |
| Bothkennar clay | 0.35 | 0.5 | 1 |

**Table S5** Typical parameters of the intergranular strain concept for clays

| Soil | $R$ | $m_R$ | $m_T$ | $\beta_r$ | $\chi$ |
|---|---|---|---|---|---|
| London clay (Mašín, 2005) | 1.e-4 | 4.5 | 4.5 | 0.2 | 6 |
| London clay (data Gasparre) | 5.e-5 | 9 | 9 | 0.1 | 1 |
| Brno clay (nat.) | 1e-4 | 16.75 | 16.75 | 0.2 | 0.8 |

**Parameters:**

- Parameter 1 – critical state friction angle $\phi_c$
- Parameter 2 – $p_t$ – shift of the mean stress due to cohesion. The effective stress $\boldsymbol{\sigma}$ used in the model formulation is replaced by $\boldsymbol{\sigma} - \mathbf{1}p_t$. Non-zero value of $p_t$ is needed to overcome problems with stress-free state. If $p_t = 0$, it will be replaced by a default value of 10 kPa. Any other value can be input by user (for basic model, set $p_t$ to very low number, e.g. $p_t = 1.e-5$)
- Parameters 3-6 – parameters of the basic hypoplastic model for clays $\lambda^*$, $\kappa^*$, $N$, $r$
- Parameters 7-9 – parameters of the unsaturated soil part of the model ($n$, $l$ and $m$)
- Parameters 10 – air entry (expulsion) value of suction $s_e$ (hydraulic hysteresis not considered in the present implementation)
- Parameter 11 – initial void ratio $e$ or overconsolidation ratio $OCR$. If $Par(16) < 10$, then $e = Par(16)$. If $Par(16) > 10$, then $OCR = Par(16) - 10$

**State variables:**

The routine uses 6 state variables:

- State v. 1 – void ratio $e$
- State v. 2 – suction $s$
- State v. 3 – Degree of saturation $S_r$
- State v. 4 – Number of evaluation of the constitutive model in one global time step (for postprocessing only)
- State v. 5 – Mobilized friction angle $\phi_{mob}$ in degrees (for postprocessing only)
- State v. 6 – Suggested size of the first time substep (for calculation control)

The hypoplastic model for unsaturated soils is implemented via user define subroutine usermod.dll. To use the model in PLAXIS, copy the file UsrMod.dll into the PLAXIS installation directory. Then, select "user-defined model" from the Material model combo box in the General tab sheet. After selecting the user-define model, correct user-define

dynamic library (typically UsrMod.dll) needs to be selected in the "Available DLL's" combo box under "Parameters" tab sheet. In the "Models in DLL" combo box, model with ID 3 (Hypoplastic-unsat.) must be selected. The parameters can then be input into the parameter table.

Typical parameters of the hypoplastic model for unsaturated soils are given in Table S6.

**Table S6** Typical parameters of the hypoplastic model for unsaturated soils

| Soil | $\phi_c$ | $\lambda^*$ | $\kappa^*$ | $N$ | $r$ | $n$ | $l$ | $m$ | $s_e$ [kPa] |
|---|---|---|---|---|---|---|---|---|---|
| Pearl clay [13] | 29◦ | 0.05 | 0.005 | 1.003 | 0.5 | 0.164 | 0.024 | 2 | 15 |
| Jossigny silt [2] | 36◦ | 0.09 | 0.0025 | 0.925 | 0.03 | 0.055 | 0 | 2 | 10 |
| Bourke silt [14] | 29.5◦ | 0.06 | 0.002 | 0.772 | 0.2 | 0.0035 | 0 | 2.5 | 18 |

# 2.5 Troubleshooting

Although the implementation has been tested to be accurate and robust, the hypoplastic models are highly non-linear which may cause problems during solving complex boundary value problems. When encountering problems, the following steps may help to improve the overall performance:

1. In the "Iterative procedure" settings under "Parameters" Tab sheet, set "Manual settings" and do not use the arc-length control.

2. Try to modify the iterative procedure by decreasing the "Desired minimum" and "Desired maximum" number of iterations (for example, 3 and 5 respectively).

3. The hypoplastic models are undefined in the tensile stress region, which can cause integration problems in the vicinity of the free surface and in the case of staged construction starting from the stress-free state. For this reason, artificial cohesion is introduced in the model implementation through the parameter $p_t$. The user can specify any $p_t$ value; in the case $p_t$=0 kPa, however, the program replaces it by a default value $p_t$=10 kPa, which is sufficient to overcome most problems due to the zero stress state.
4. When used with interface elements, proper interface parameters must be input in the "Interface" Tab sheet under "Material models" window. Particularly, as some tensile stress is allowed for in the soil through the parameter $p_t$, the tensile stress should be allowed for also in the interface by increasing the cohesion value (e.g., 10 kPa). Convergence problems may also be caused by high interface stiffness. In the case PLAXIS keeps on iterating although the global error is below the tolerated value, or does not increase the step size although the number of iterations is below the "desired minimum", problem is the most likely in interfaces.

# 2.6 Evaluation

## 2.6.1 Drained triaxial test

PLAXIS implementation of the hypoplastic models has been evaluated by means of simulations of a drained triaxial test. Fig. S14 shows the stress-strain curves of the drained triaxial test, compared with "exact" results obtained by accurate time integration of the model using a single-element program. The curves generated by the PLAXIS implementation practically coincide with the "exact" solution.

## 2.6.2 Submerged construction of an excavation

In this case, submerged construction of an excavation close to the river is simulated. The upper 20 m of the subsoil consist of soft soil layers, which are modeled as a single homogeneous clay layer using the clay hypoplastic model. Underneath this clay layer there is a stiffer sand layer, modeled using the sand hypoplasticity model. As in this case the displacement field is significantly influenced by the small-strain behavior, hypoplastic models with the intergranular strain concept are used.

Soil parameters of the sand layer correspond to the Hochstetten sand from Tab. S1; the intergranular strain parameters used are in Tab. S2. The sand is in a medium dense state with $e_0$=0.7. The clay layer is simulated with London clay parameters (Tab. S3 for parameters of the basic model; Tab S5. for the intergranular strain parameters), with the initial value of OCR equal to 2.

Figure S15 shows the displacement field and Fig. S16 shows the normalized length

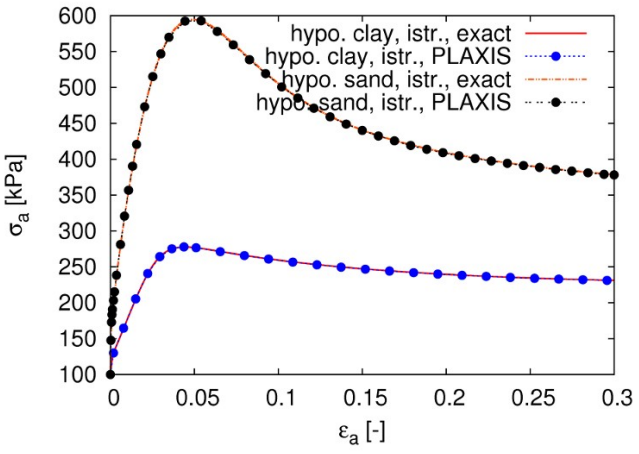


**Figure S14** Stress-strain curves of the drained triaxial test for the sand and clay hypoplastic models with the intergranular strain concept compared with the "exact" solution of the intergranular strain tensor.

The normalized length of the intergranular strain tensor varies between 0, which indicates the soil being inside the elastic range, and 1, corresponding to the state swept-out of the small-strain memory. In the case of the normalized length of the intergranular strain being equal to 1 the soil behavior is governed by the basic hypoplastic model. Indeed, Fig. S16 shows that this is the case of the submerged construction of an excavation, where the soil is below the bottom of the excavation and behind the wall outside the small-strain-stiffness range.

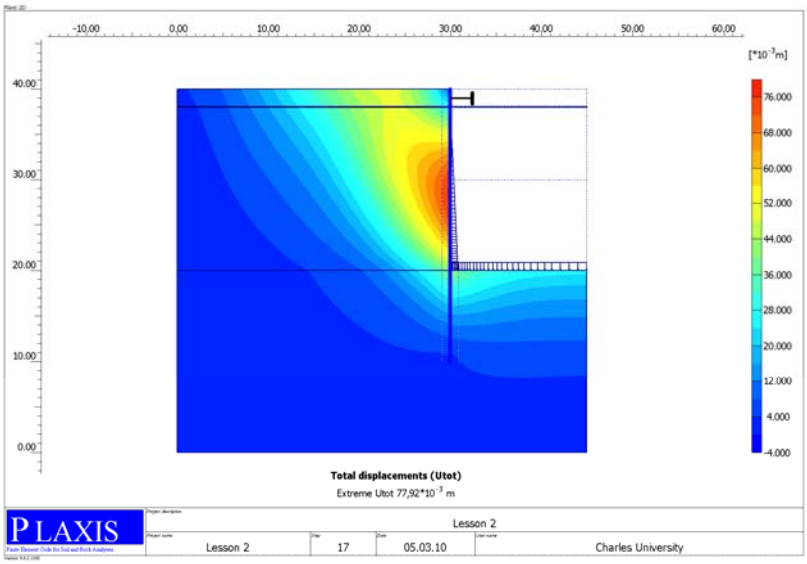


**Figure S15** Submerged construction of an excavation – total displacement

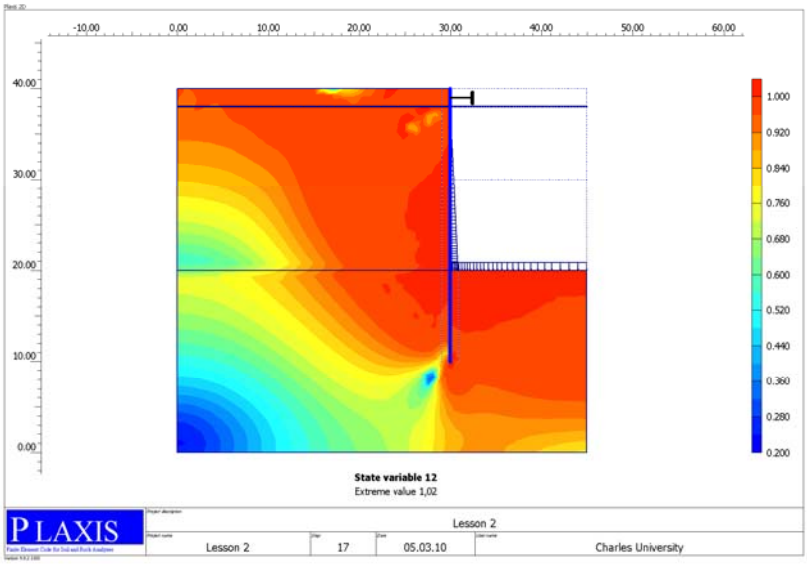


**Figure S16** Submerged construction of an excavation – normalized length of the intergranular strain tensor

### 2.6.3 Settlement due to tunnel construction

In the next example, a shield tunnel excavated partly in soft clay and partly in medium dense sand is simulated, and its influence on a pile foundation is evaluated. The tunnel has a diameter of 5 m and is located at an average depth of 20 m. The soil profile indicates four distinct layers: The upper 13 m consists of soft clay type soil. Under the clay layer there is a 2 m thick sand layer, which is used as a foundation layer for the piles. Below this sand layer, there is another clay layer followed by a deep sand deposit.

As in the previous example, soil parameters of the sand layer correspond to the Hochstetten sand from Tab. S1; the intergranular strain parameters used are in Tab. S2. The sand is in a medium dense state with $e_0$=0.7. The clay layer is simulated with London clay parameters (Tab. S3 for parameters of the basic model; Tab S5. for the intergranular strain parameters), with the initial value of OCR equal to 2.

Figure S17 shows the displacement field and Fig. S18 shows the normalized length of the intergranular strain tensor. Again, the normalized length of the intergranular strain tensor in Fig. S18 demonstrates how the small-strain stiffness is activated in different parts of the modeled geometry. The soil is in "hypoplastic" state in the vicinity of the tunnel, above the tunnel and also next to the pile foundations, which bear the building weight. Further from the tunnel, the value of the normalized length of the intergranular strain tensor is low and at these places the soil remains elastic with high shear and bulk stiffnesses.

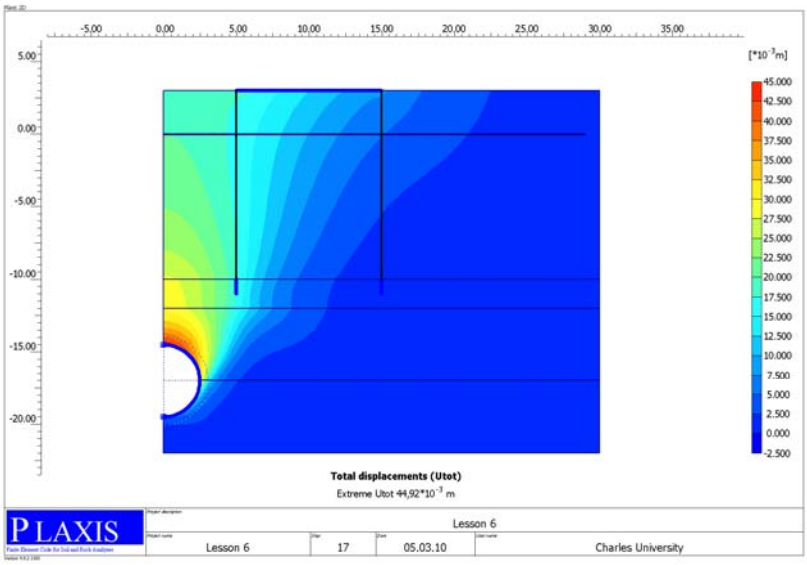


**Figure S17** Settlement due to tunnel construction – total displacement.

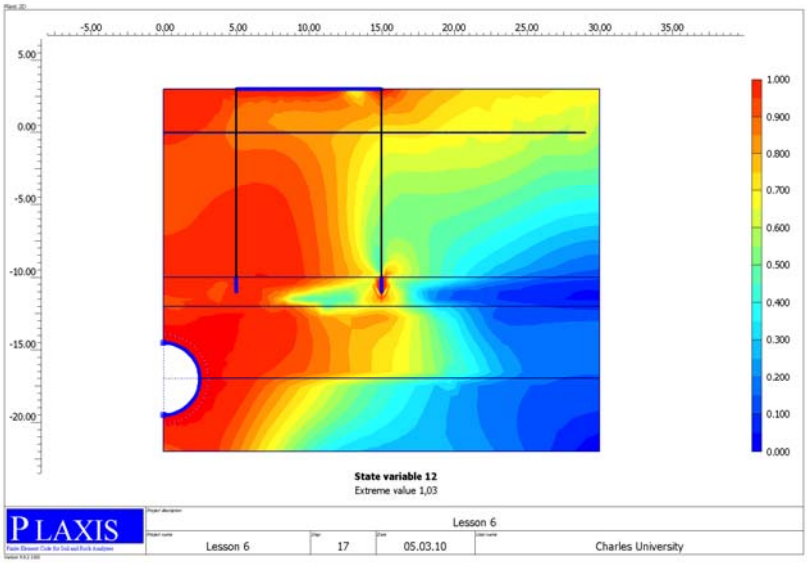


**Figure S18** Settlement due to tunnel construction, normalized length of the intergranular strain tensor.

## 2.6.4 Building subjected to an earthquake

This example demonstrates capabilities of a hypoplastic model in dynamic analysis of the earthquake impact on existing infrastructure. A real accelerogram of an earthquake recorded by USGS in 1989 is used for the analysis.

The building consists of 4 floors and a basement. It is 6 m wide and 25 m high. The subsoil consists of a sand with water level reaching the surface. The soil behavior during the earthquake is considered as undrained. Two cases were simulated. In one case, the soil is in a loose state ($e_0 = e_{c0}$), in the second case the soil is in a dense state ($e_0$ is close to $e_{d0}$). Hypoplastic model parameters of the Hochstetten sand from Tab. S1 and the intergranular strain parameters from Tab. S2 are adopted.

Overall displacements of the top of the building are shown in Fig. S19. The soil response to the earthquake depends significantly on the soil state. The loose soil liquefied after 3-4s of the earthquake, leading to the failure. The analysis cannot continue and fails. The displacements are much lower in the case of dense soil. Although some displacements occur also in this case, the soil retains some bearing capacity sufficient to overcome the failure.

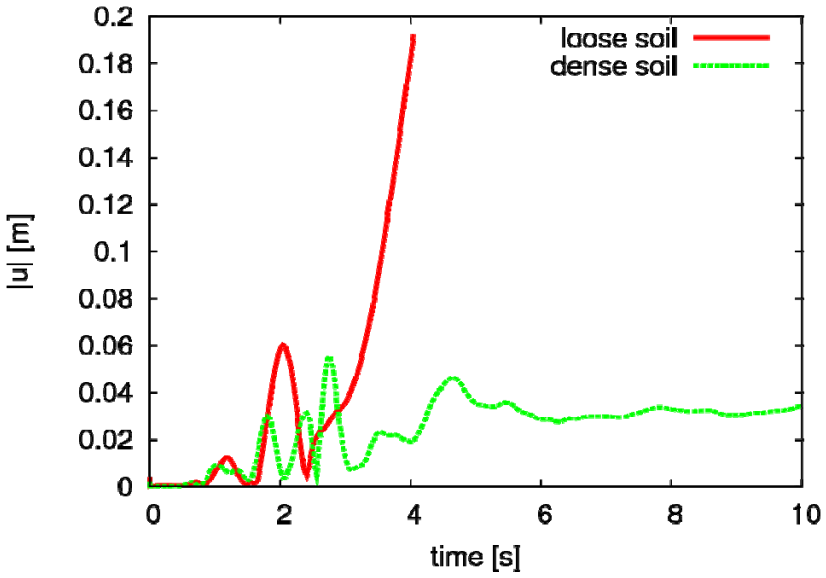


**Figure S19** Displacement of the top of the building during the earthquake

Figure S20 shows total displacements after approximate 4 s of earthquake for the loose soil case, whereas Figure S21 shows the displacements at the same time (and in the same scale) for the dense soil. The figure indicates foundation failure for the loose soil case and relatively low displacements for the dense soil case.

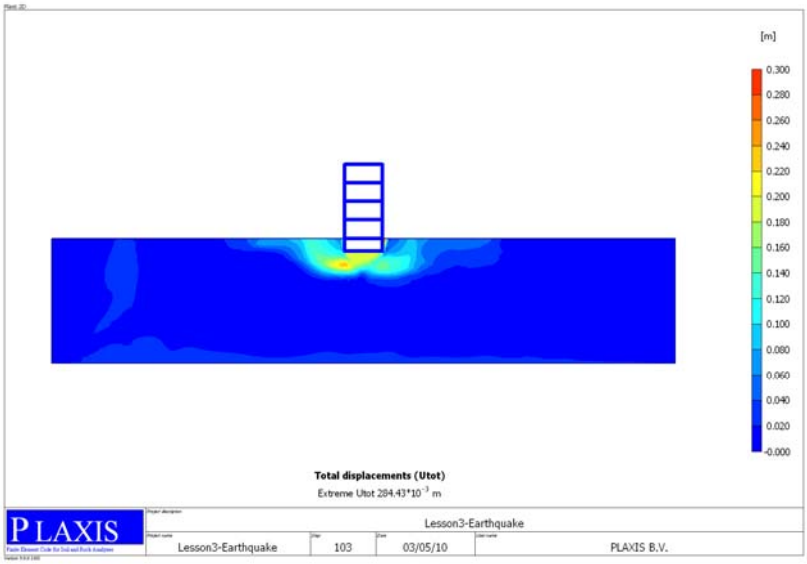


**Figure S20** Total displacements after 4 s of earthquake – loose soil

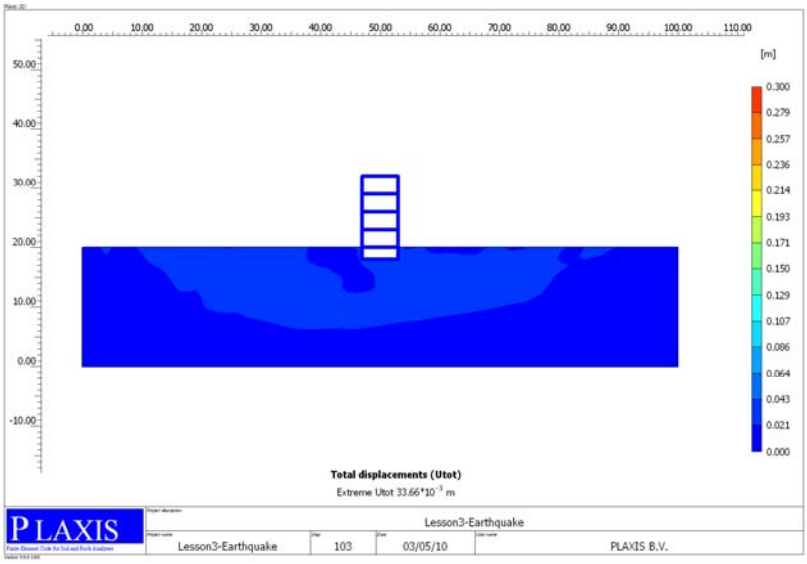


**Figure S21** Total displacements after 4 s of earthquake – dense soil

## 2.6.5 Wetting-induced collapse of a foundation

This example is taken over and modified from Galavi (2010). It describes simulation of stiff footing on a partially saturated soil which collapses on wetting. The fully coupled flow-deformation analysis is applied. Soil behavior is described using the hypoplastic model for unsaturated soils (parameters are in Tab. S7). Figure S22 shows the FE mesh and the boundary conditions used for the analysis. The mesh consists of 293 numbers of 15-noded triangular elements with a fourth order interpolation for displacements and for pore pressures and 12 Gauss points (stress points) for each element. The width of the model is 10 m and height 11 m and a distributed load with width of 2 m is applied to simulate foundation load. Foundation is simulated using beam element. The initial position of phreatic line is on the surface. This level is changed during drying and wetting processes.

**Table S7** Parameters of the hypoplastic model for unsaturated soils used in the simulation

| $\phi_c$ | $\lambda^*$ | $K^*$ | $N$ | $r$ | $n$ | $l$ | $m$ | $s_e$ [kPa] | $OCR_0$ |
|---|---|---|---|---|---|---|---|---|---|
| 20° | 0.1 | 0.01 | 1 | 0.5 | 0.05 | 0 | 2 | 10 | 2 |

In this example, soil is dried so that the suction reaches 100 kPa at the surface nodes and then the footing is vertically loaded to 150 kPa. After this loading phase, the soil is imposed to wetting. The top, left and right boundaries are closed for flow, and drying and wetting are only applied through the bottom boundary by linearly changing the water head in time (in drying phase, the head reduces from 10 m to 0 and in wetting phase the head increases to 8.5 m). All phases are performed slowly in order to maintain drained conditions (in 1000 days). The value of suction before and after wetting is in Fig. S23

Figures S22 (deformation), S24 (volumetric strain) and S25 (shear strain) show results of the coupled flow-deformation analysis. After the foundation load, the foundation centre settles by 28.6 cm, whereas far-field surface point settles by 0.8 cm. After wetting, total deformation of foundation center is -118.9 m, whereas total deformation of far field surface point is +0.8

cm. Therefore, during wetting, the soil below foundation collapses (additional settlement 118.1 cm), whereas heave is observed in the far field (1.6 cm). Contour plot of volumetric strains shows the volumetric de- formation is localized below the foundation (Fig. S24). Contour plot of shear strain (Fig. S25) demonstrates that the soil undergoes not only volumetric collapse due to wetting, but also shear displacements due to decrease of a soil strength.

The mechanism controlling the predicted response is governed by the actual overconsolidation ratio. Soil in the far field remains even after application of the foundation load in overconsolidated conditions (initial OCR=2), it thus suffers volumetric heave implied by the suction decrease (response is governed by the decrease of effective stress). Contrary, the soil below foundation has been loaded to a state close to its normally consolidated conditions. Such a soil undergoes wetting induced collapse, due to decrease of the state boundary surface size.

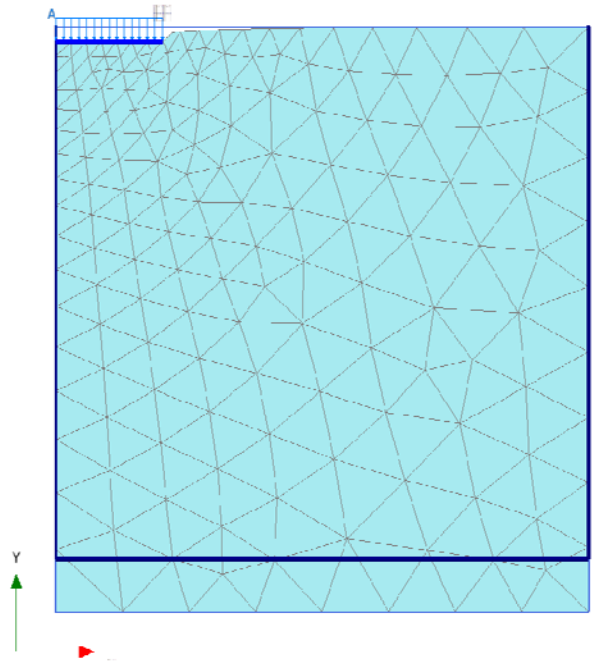


**Deformed mesh |u| (at true scale)**

Maximum value = 0,2862 m (Element 12 at Node 640)

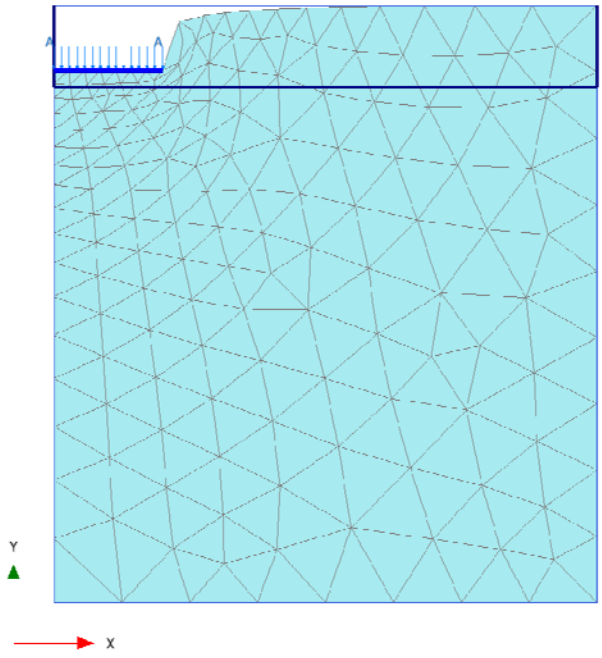


**Deformed mesh |u| (at true scale)**

Maximum value = 1,189 m (Element 12 at Node 640)

**Figure S22** Deformed mesh after foundation load (upper) and after wetting (lower)

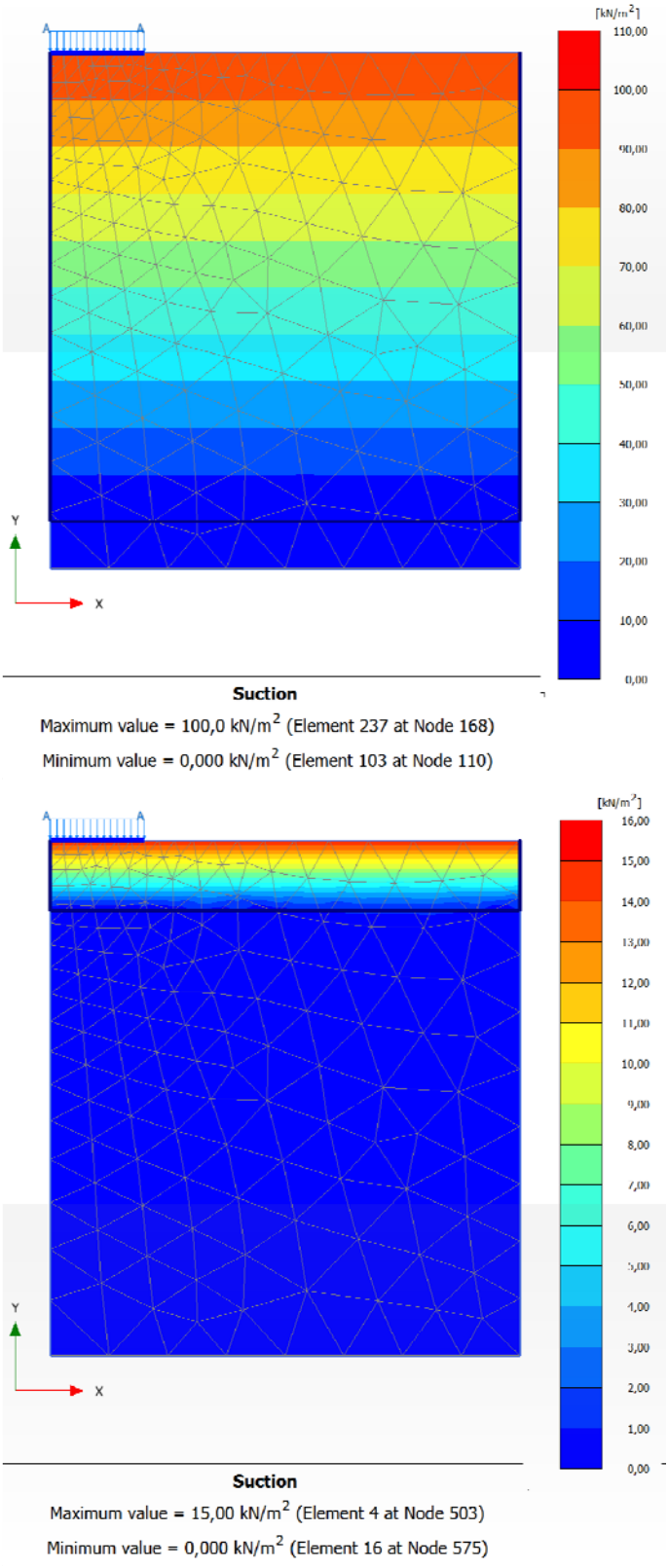


**Figure S23** Suction during foundation load (upper) and after wetting (lower)

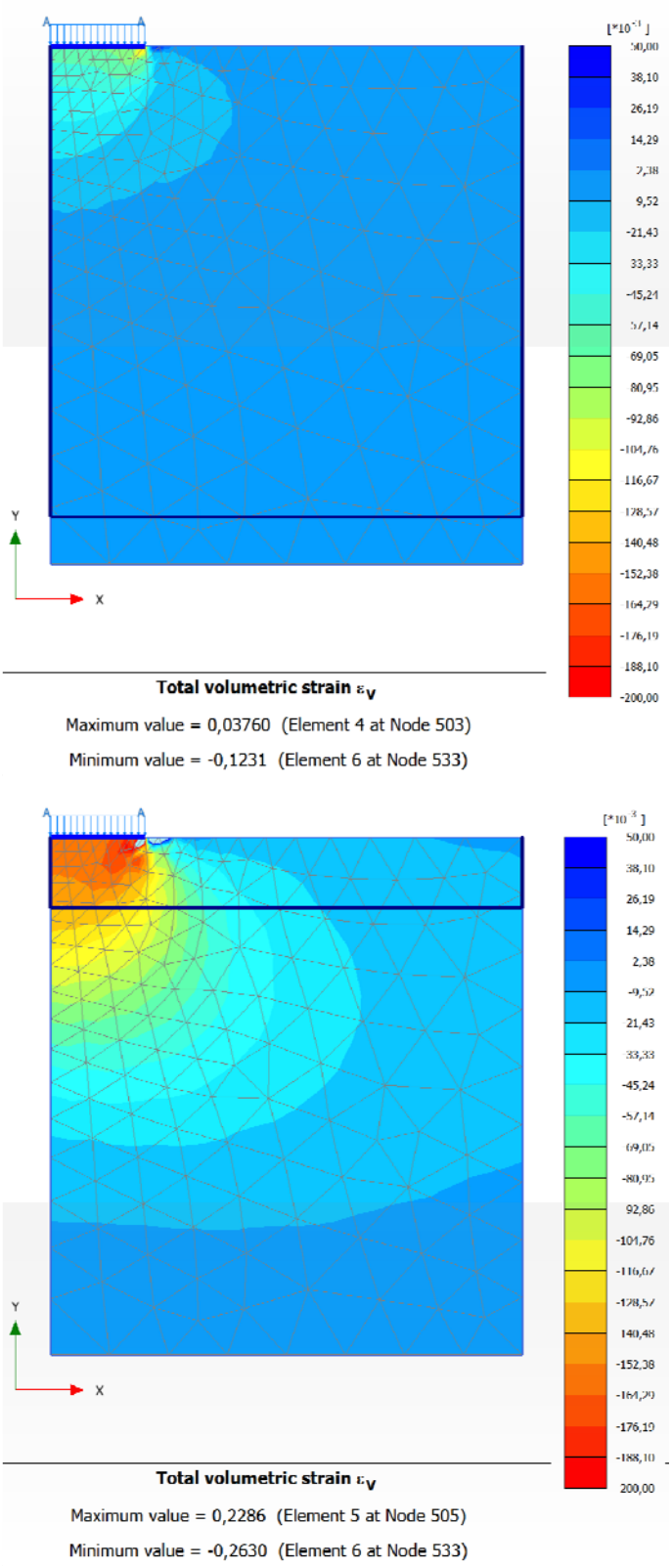


**Figure S24** Volumetric strain after foundation load (upper) and after wetting (lower)

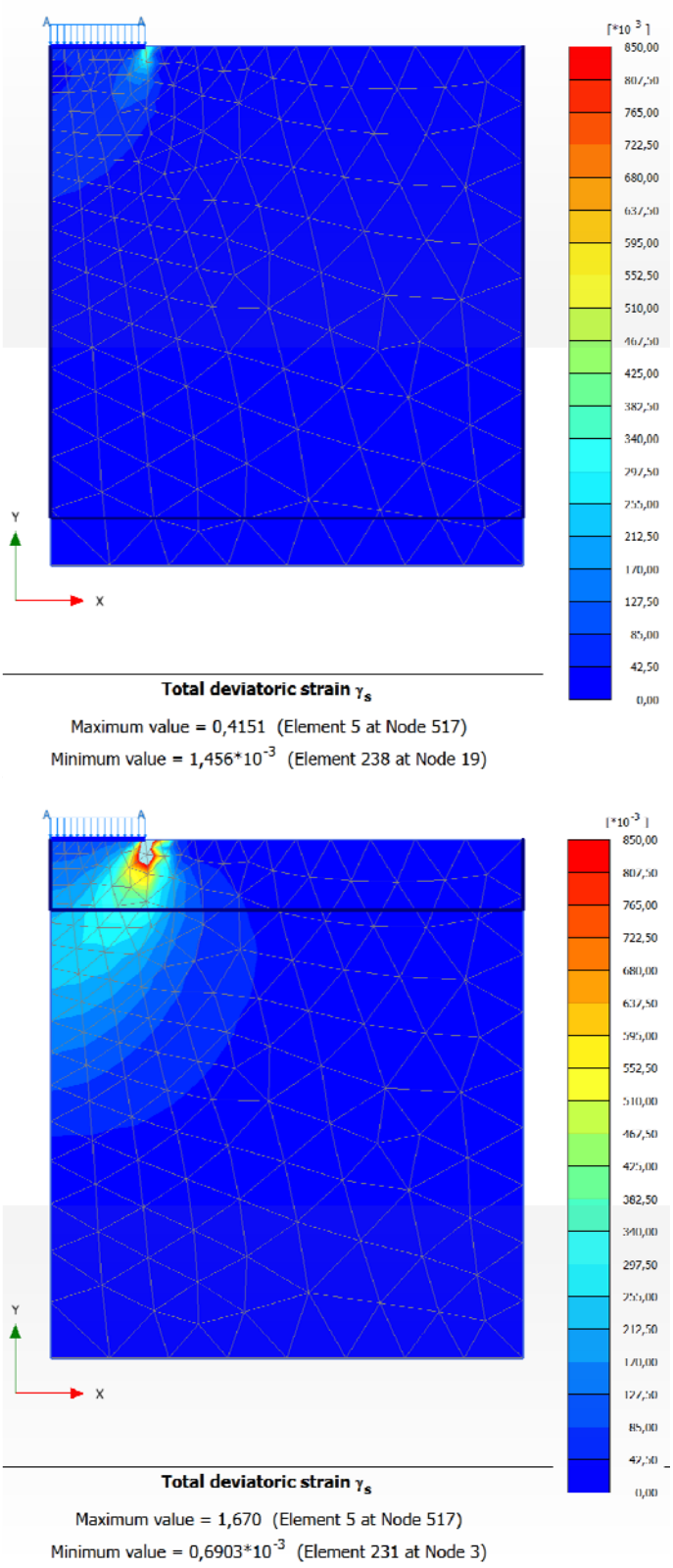


**Figure S25** Shear strain after foundation load (upper) and after wetting (lower)

# Acknowledgement

The RKF-23 time integration scheme was programmed and kindly provided by Prof. C. Tamagnini and E. Sellari. The original umat-PLAXIS interface, which served as a basis for the present developments, was programmed and kindly provided by Dr. P.-A. von Wolffersdorff. The implementation was optimized during the stay of the author at Plaxis bv in March 2010. Plaxis support is greatly appreciated. The implementation was partly supported by the research grants GACR 205/08/0732 and MSM 0021620855.

# CHAPTER 3
# DETERMINATION OF HYPOPLASTICITY MODEL PARAMETERS

## 3.1 Introduction

This chapter describes details of hypoplasticity model parameters determination in the manuscript entitled "Effects of pillar depth and shielding on the interaction of crossing multitunnels". Procedures of model parameter calibration are given and the result of calibration is shown in this document.

## 3.2 Model Parameters

Hypoplasticity model requires total 13 parameters. The parameters can be divided into two groups, the basic model and small strain stiffness parameters. The basic hypoplasticity model requires eight material parameters ($\phi_c$, $h_s$, n, $e_{d0}$, $e_{c0}$, $e_{i0}$, $\alpha$, $\beta$). Parameter $\phi_c$ is the critical state friction angle, which can be calibrated using the angle of repose test. The parameters $h_s$ and n describe the slope and shape of limiting void ratio lines; that is, isotropic normal compression line, critical state line and minimum void ratio line. Parameters $e_{d0}$, $e_{c0}$ and $e_{i0}$ specify positions of these lines in the mean stress versus void ratio diagram. The parameters $h_s$, n and $e_{c0}$ can be calibrated using oedometric test on loose sand sample. The parameters $e_{d0}$ and $e_{i0}$ can typically be estimated using empirical correlations. Finally, the model requires parameter $\alpha$ specifying peak friction angle and parameter $\beta$ specifying shear stiffness. These parameters can be estimated using triaxial shear test.

The intergranular strain formulation or small strain stiffness requires five additional parameters, namely $m_R$, $m_T$, R, $\beta_r$ and $\chi$. Parameters $m_R$ and $m_T$ specify very small strain shear stiffness upon 180° and 90° change of strain path direction, respectively. Parameter R specifies the size of elastic range measured in the strain space; $\beta_r$ and $\chi$ specify the rate of stiffness degradation with strain.

## 3.3 Determination of Model Parameters

Hypoplasticity model parameters for large strain behavior or basic model parameters ($\phi_c$, $h_s$, n, $e_{c0}$, $e_{d0}$, $e_{i0}$,) for Toyoura sand were adopted based on calibration resulted proposed by Herle and Gudehus (1999). Exponent $\alpha$, exponent $\beta$ and small strain stiffness or intergranular strain concept parameters ($m_R$, $m_T$, R, $\beta_r$ and $\chi$) were calibrated using the curve fitting method. In this study, the computed results were fitted to triaxial test with local strain measurement results from Yamashita et al. (2000) and bender element tests from Yamashita el al. (2009). The model parameters were summarized in Table 1. Detailed calibration of each parameter is given below.

### 3.3.1 Parameter controlling behavior in large strain

Following details show determination criteria for parameters controlling behavior in large strain range, which consist of $\phi_c$, $h_s$, n, $e_{c0}$, $e_{d0}$, $e_{i0}$, $\alpha$, $\beta$.

**$\phi_c$**: Critical state friction angle
Calibration: perform angle of repose test or shear test

**$h_s$**: Parameter controlling the overall slope of limiting void ratio curves
**n**: Parameter controlling curvature of limiting void ratio curves
**$e_{c0}$**: Parameter controlling position of initial critical state void ratio
**$e_{i0}$**: Parameter controlling isotropic compression line or the theoretical loosest possible state
**$e_{d0}$**: Parameter controlling minimum void ratio or the densest state void ratio

Equation S9 shows the relationship of $h_s$, n, $e_{c0}$, $e_{d0}$ and $e_{i0}$ shows limiting void ratio curves:

$$\frac{e_i}{e_{i0}} = \frac{e_c}{e_{c0}} = \frac{e_d}{e_{d0}} = \exp\left[-\left(\frac{3p'}{h_s}\right)^n\right] \quad \text{(S9)}$$

Calibration: carry out oedometric test or isotropic triaxial test
n can be calibrated by oedometric loading test of an initially loose sample as shown in Equation S10:

$$n = \frac{\ln(e_{p1}C_{c2} / e_{p2}C_{c1})}{\ln(p_{s2} / p_{s1})} \quad \text{(S10)}$$

$h_s$ can be calculated based on relationship between $h_s$ and n as shown in Equation 3:

$$h_s = 3p_s\left(\frac{ne_p}{C_c}\right)^{1/n} \quad \text{(S11)}$$

Calibration: perform shear test or index test to determine minimum and maximum density and cyclic shearing test

$e_{c0}$ can be obtained from a shear test on a soil element at the same time as the calibration of critical state friction angle ($\phi_c$) or from a relationship between $e_{c0}$ and $e_{max}$ from an index test using Equation S12:

Empirical relationship $e_{c0} = e_{max}$ (Herle and Gudehus, 1999) (S12)

$e_{d0}$ can be obtained by cyclic shearing test with small amplitude under constant pressure or adopted from an empirical relationship with $e_{c0}$ or from an index test (Equations S13 and S14):

Empirical relationship $e_{d0} = 0.5\ e_{c0}$ (Herle and Gudehus, 1999) (S13)

Empirical relationship $e_{d0} = e_{min}$ from an index test (S14)

$e_{i0}$ can be calculated from idealized packing of spheres and cubes. It is not practical to obtain $e_{i0}$ from experimental and it is often related to an empirical relationship with $e_{c0}$ in Equation S15.

Empirical relationship $e_{i0} = 1.2\ e_{c0}$ (Herle and Gudehus, 1999) (S15)

The controlling void ratio curves for Toyoura sand using parameters in Table S8 are shown in Figure S26.

$\alpha$: Parameter controlling the dependency of peak friction angle on relative density
$\beta$: Parameter controlling the dependency of soil stiffness on relative density

Calibration: conduct drained triaxial shear test
Parameter $\alpha$ can be calculated based on relationship between $\phi_p$, $\phi_c$, e, $e_d$ and $e_c$.
Parameter $\beta$ can be calculated based on relationship between e, $e_{c0}$, $e_{d0}$, $E_{dense}$ and $E_{loose}$.
Alternative calibration: curve fitting $\alpha$ and $\beta$ to results of drained triaxial shear test using numerical soil testing software such as PLAXIS 3D (Brinkgreve et al, 2013) "Soil test" utility.

### 3.3.2 Small strain stiffness parameters

Small strain stiffness or intergranular strain parameters consist of following details.
$\mathbf{m_R}$: Parameter controlling the shear modulus of initial loading (very small strain) or upon 180° strain path reversal (i.e., $m_R$ controls $G_0$)
$\mathbf{m_T}$: Parameter controlling the shear modulus upon 90° strain path reversal
**R**: Parameter controlling the size of the elastic range
$\beta_r$: Parameter controlling the intergranular strain evolution rate
$\chi$: Parameter controlling the tangent stiffness degradation with normalized length of intergranular strain tensor ($\rho$)

Calibration: perform drained triaxial shear test on sample using local strain measurement then calibrate $m_R$, $m_T$, R, $\beta_r$ and $\chi$ by means of fittings to the element test results
Empirical relationship $m_T = 0.5\ m_R$ (Atkinson et al., 1990)

# 3.4 Numerical Calibration Result

Figure S27 shows a comparison between measured and computed secant modulus Young's modulus of Toyoura sand (Yamashita et al., 2000, 2009). Element tests from Yamashita et al. (2000) were carried out by using drained triaxial compression test with local strain measurement. In addition, a result of secant shear modulus (G) of Toyoura sand obtained from Yamashita et al. (2009) was converted into $E_s$ as a comparison in the small strain range. The soil sample tested in this figure was prepared by anisotropic consolidation ($K_0 = 0.46$) on reconstituted dry pluvial deposition method, which is the same method adopted to prepare soil sample in the centrifuge test. The void ratio of sand and confining pressure in Yamashita et al. (2000) were 0.799 and 46 kPa, respectively. The computed result was carried out by using "Soil test" utility in PLAXIS 3D 2013 (Brinkgreve et al, 2013). The parameters controlling behavior in large strain (i.e., $\phi_c$, $h_s$, n, $e_{c0}$, $e_{d0}$, $e_{i0}$) were adopted from Herle and Gudehus (1999). Exponents $\alpha$ and $\beta$ were fitted to triaxial test result with local strain

measurement presented by Yamashita et al. (2000). Initial secant modulus or very small strain modulus was fitted by controlling $m_R$. Parameter $m_T$ was assumed to be $0.5m_R$ based on Atkinson et al. (1990). Parameters R and $\chi$ were assumed to be material independent constants as $3x10^{-5}$ and 1, respectively. Thus, secant modulus degradation curve was fitted by controlling $\beta_r$. Intergranular strain concept parameters adopted in this study were within the range reported in previous studies (Niemunis and Herle, 1997).

**Table S8** Summary of material parameters adopted in finite element analyses

| | |
|---|---|
| Critical state friction angle, $\phi_c$ | 30° |
| Granulates hardness, $h_s$ | 2.6 GPa |
| Exponent n, n | 0.27 |
| Minimum void ratio at zero pressure, $e_{do}$ | 0.61 |
| Critical void ratio at zero pressure, $e_{co}$ | 0.98 |
| Maximum void ratio at zero pressure, $e_{io}$ | 1.10 |
| Exponent $\alpha$, $\alpha$ | 0.5 |
| Exponent $\beta$, $\beta$ | 3 |
| Parameter controlling the initial shear modulus upon a 180° strain path reversal and in the initial loading, $m_R$ | 8 |
| Parameter controlling the initial shear modulus upon a 90° strain path reversal, $m_T$ | 4 |
| The size of the elastic range, R | 0.00003 |
| Parameter controlling the rate of degradation of stiffness with strain, $\beta_r$ | 0.2 |
| Parameter controlling the rate of degradation of stiffness with strain, $\chi$ | 1.0 |

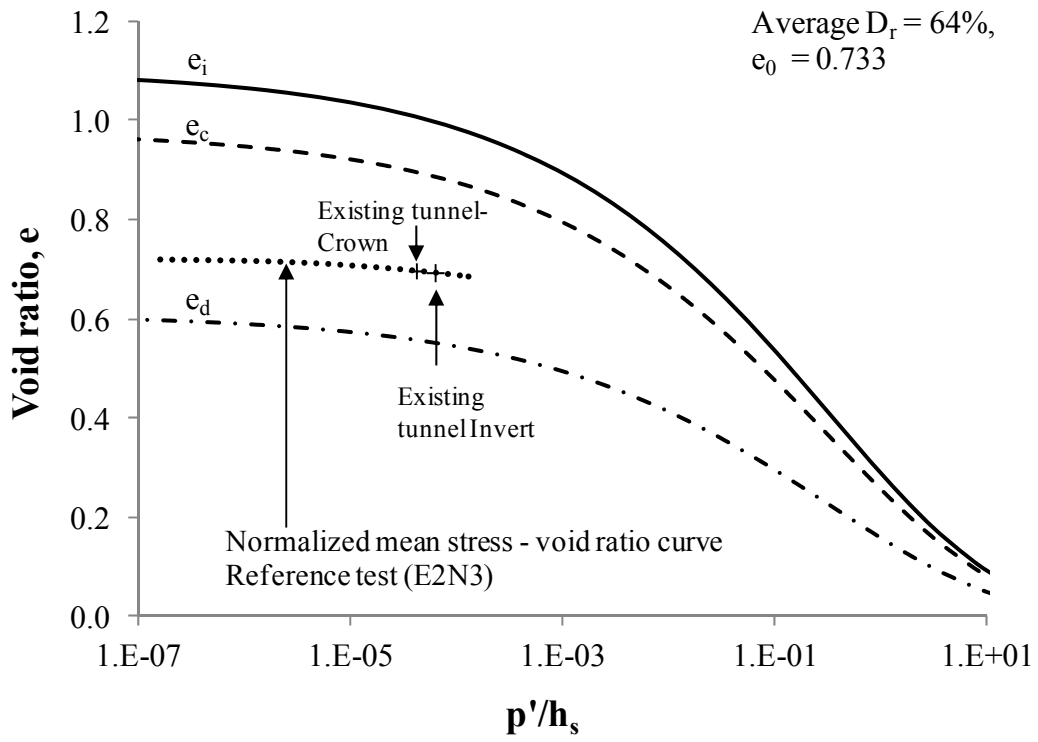


**Figure S26** Controlling void ratio curves for Toyoura sand

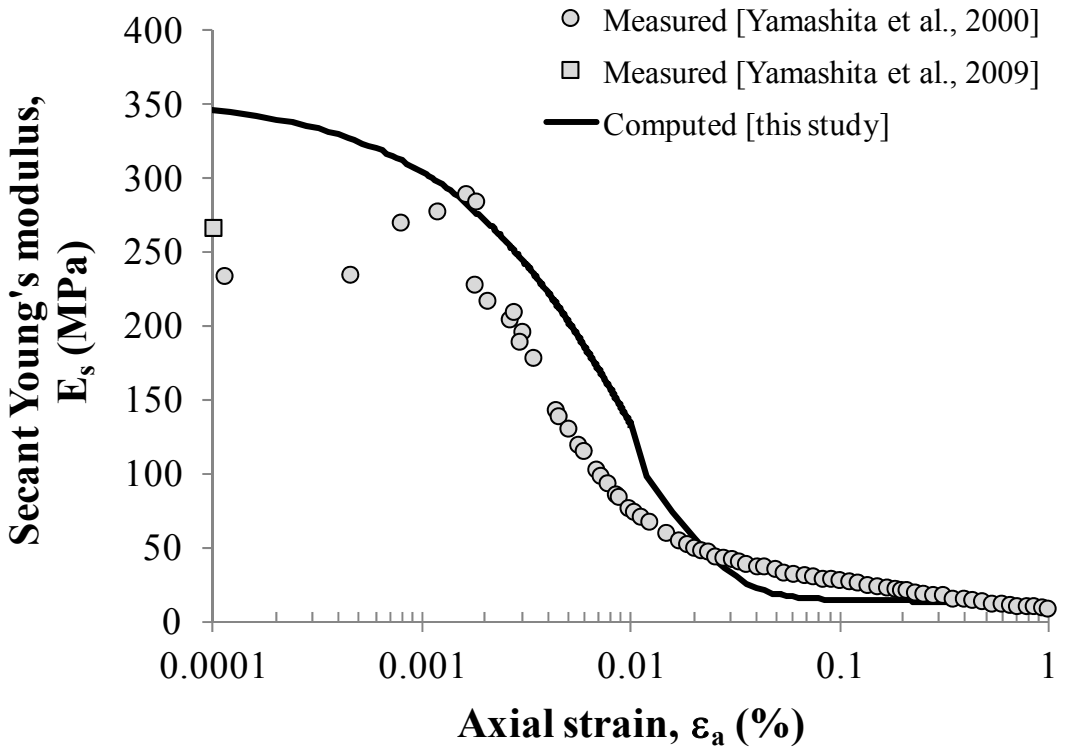


**Figure S27** Calibration of parameters with test results with bender element and local strain measurement

# REFERENCES


Atkinson, J. H., Richardson, D., Stallebrass, S. E. (1990). "Effect of stress history on the stiffness of overconsolidated soil." *Géotechnique*, 40(4), 531-540.

Bauer, E. (1996). Calibration of a comprehensive constitutive equation for granular materials. *Soils and Foundations*, 36(1),13–26.

Brinkgreve, R. B. J., Engin, E. and Swolfs, W. M. (2012). *PLAXIS 3D 2012 User manual*. Plaxis BV, Delft, The Netherlands

D'Onza, F., Gallipoli, D., Wheeler, S., Casini, F., Vaunat, J., Khalili, N., Laloui, L., Mancuso, C., Mašín, D., Nuth, M., Pereira, M., and Vassallo, R. (2011). Benchmark of constitutive models for unsaturated soils. *Géotechnique*, 61(4), 283–302.

Galavi, V. (2010). *Groundwater flow, fully coupled flow deformation and undrained analyses in PLAXIS 2D and 3D*. Technical report, Plaxis BV 2010, research department

Garnier, J., Gaudin, C., Springman, S. M., Culligan, P. J., Goodings, D. König, D., Kutter, B., Phillips, R., Randolph, M. F. and Thorel, L. (2007). "Catalogue of scaling laws and similitude questions in geotechnical centrifuge modeling." *International Journal of Physical Modelling in Geotechnics,* 3, 1-23.

Gasparre, A. (2005). *Advanced laboratory characterisation of London Clay*. PhD thesis, University of London, Imperial College of Science, Technology and Medicine

Gudehus, G. (1996) A comprehensive constitutive equation for granular materials. *Soils and Foundations*, 36(1), 1–12.

Herle, I. and Gudehus, G. (1999). "Determination of parameters of a hypoplastic constitutive model from properties of grain assemblies." *Mechanics of cohesive-frictional materials,* 4, 461-486.

Herle, I. and Kolymbas, D. (2004). Hypoplasticity for soils with low friction angles. *Computers and Geotechnics*, 31(5), 365–373.

Ishihara, K. (1993). "Liquefaction and flow failure during earthquakes." *Géotechnique*, 43(3), 351-415.

Kolymbas, D. (1991). Computer-aided design of constitutive laws. *International Journal for Numerical and Analytical Methods in Geomechanics*, 15, 593–604.

Mašín, D. (2005). A hypoplastic constitutive model for clays. *International Journal for Numerical and Analytical Methods in Geomechanics*, 29(4), 311–336.

Mašín, D. (2007). A hypoplastic constitutive model for clays with meta-stable structure. *Canadian Geotechnical Journal*, 44(3), 363–375.

Mašín, D. (2009). 3D modelling of a NATM tunnel in high K0 clay using two different constitutive models. *Journal of Geotechnical and Geoenvironmental Engineering ASCE*, 135(9), 1326–1335.

Mašín, D. (2010). Hypoplasticity for practical applications – PhD course. http://web.natur.cuni.cz/uhigug/masin/hypocourse

Mašín, D. and N. Khalili (2008). A hypoplastic model for mechanical response of un-saturated soils. *International Journal for Numerical and Analytical Methods in Geomechanics*, 32(15), 1903–1926.

Mašín, D. and N. Khalili. (2011) A thermo-mechanical model for variably saturated soils

based on hypoplasticity. *International Journal for Numerical and Analytical Methods in Geomechanics,* 36(12), 1461–1485.

Niemunis, A. (2002). *Extended Hypoplastic Models for Soils*. Habilitation thesis, Ruhr-University, Bochum

Niemunis, A. and Herle, I. (1997). "Hypoplastic model for cohesionless soils with elastic strain range." *Mechanics of cohesive-frictional materials*, 2, 279-299.

Todd, C. D. (1975). *The potentiometer handbook*. McGraw-Hill, New York.

von Wolffersdorff, P. A. (1996) A hypoplastic relation for granular materials with a predefined limit state surface. *Mechanics of Cohesive-Frictional Materials*, 1, 251–271.

Yamashita, S., Jamiolkowski, M. and Lo Presti, D.C.F. (2000). "Stiffness nonlinearity of three sands." *J. Geotech. Geoenviron. Engng*., 126(10), 929-938.

Yamashita, S., Kawaguchi, T., Nakata, Y., Mikami, T., Fujiwara, T. and Shibuya, S. (2009). "Interpretation of international parallel test on the measurement of $G_{max}$ using bender elements." *Soils Found.,* 49(4), 631–650.